Battle for the EF-Hands: Magnesium−Calcium Interference in Calmodulin[†]

Anders Malmendal,*[,‡] Sara Linse, Johan Evenäs, Sture Forsén, and Torbjörn Drakenberg

Physical Chemistry 2, Lund University, P.O. Box 124, S-221 00 Lund, Sweden

Received April 23, 1999; Revised Manuscript Received July 2, 1999

ABSTRACT: The ubiquitous Ca^{2+}-regulatory protein calmodulin activates target enzymes as a response to submicromolar Ca^{2+} increases in a background of millimolar Mg^{2+}. The potential influence of Mg^{2+}/Ca^{2+} competition is especially intriguing for the N-terminal domain of the protein which possesses the sites with the lowest Ca^{2+} specificity. The interdependence of Ca^{2+} and Mg^{2+} binding in the N-terminal domain of calmodulin was therefore studied using ^{43}Ca NMR, $^{1}H-^{15}N$ NMR, and fluorescent Ca^{2+} chelator techniques. The apparent affinity for Ca^{2+} was found to be significantly decreased at physiological Mg^{2+} levels. At Ca^{2+} concentrations of an activated cell the $(Ca^{2+})_2$ state of the N-terminal domain is therefore only weakly populated, indicating that for this domain Ca^{2+} binding is intimately associated with binding of target molecules. The data are in good agreement with a two-site model in which each site can bind either Ca^{2+} or Mg^{2+}. The $Mg^{2+}-Ca^{2+}$ binding interaction is slightly positively allosteric, resulting in a significantly populated $(Mg^{2+})_1(Ca^{2+})_1$ state. The Ca^{2+} off-rate from this state is determined to be at least one order of magnitude faster than from the $(Ca^{2+})_2$ state. These two findings indicate that the $(Mg^{2+})_1$-$(Ca^{2+})_1$ state is structurally and/or dynamically different from the $(Ca^{2+})_2$ state. The ^{43}Ca quadrupolar coupling constant and the ^{1}H and ^{15}N chemical shifts of the $(Mg^{2+})_1(Ca^{2+})_1$ state were calculated from titration data. The values of both parameters suggest that the $(Mg^{2+})_1(Ca^{2+})_1$ state has a conformation more similar to the "closed" apo and $(Mg^{2+})_2$ states than to the "open" $(Ca^{2+})_2$ state.

The impact of Mg^{2+} on Ca^{2+} binding to calmodulin (CaM)[1] is of large physiological relevance and has long been a matter of debate *(1−5)*. Ca^{2+}-dependent regulation of cellular activities is achieved by transiently increasing the cytosolic Ca^{2+} concentration from less than 0.1 μM to 1−10 μM *(6, 7)*, in a milieu with a nearly constant Mg^{2+} concentration of 0.5−2.0 mM *(8)*. Since this implies that the primary protein targets of Ca^{2+} must be able to respond in a background of a 100−10 000-fold excess of Mg^{2+}, the interdependence of Mg^{2+} and Ca^{2+} binding is an issue of great importance. While Mg^{2+}-specific proteins can rely on the large excess of Mg^{2+} *(9)*, the intracellular Ca^{2+}-binding proteins, like CaM and other EF-hand proteins, need discrimination against Mg^{2+}. This may be accomplished by taking advantage of the larger ionic radius of Ca^{2+} and its less stringent demands on the number (often 6−8) and the spatial arrangement of coordinating oxygen ligands, compared to Mg^{2+} that has a strong preference for 6-fold coordination in an octahedral symmetry *(10, 11)*.

CaM consists of two distinct domains connected by a flexible tether. The two domains are structurally similar, with cooperative Ca^{2+} binding to a pair of "EF-hand" helix−loop−helix motifs *(12)* in each domain. Upon Ca^{2+} binding the secondary structural elements in both domains remain essentially unchanged while their relative orientations change, driving the protein from a "closed" to an "open" structure (Figure 1). This results in the exposure of well-defined hydrophobic patches in both domains, where targets such as self-inhibitory peptide segments of various enzymes may bind *(13−16)*. The two domain "fragments" of CaM were originally separated by trypsin cleavage in the presence of Ca^{2+} and are therefore named TR_1C and TR_2C *(17, 18)*. They can be expressed and produced independently *(19)*, fold independently *(20, 21)*, and have Ca^{2+}-binding characteristics similar to the corresponding domains in intact CaM *(22)*.

Presently, three crystal structures of Mg^{2+} bound to EF-hand proteins have been solved. In all of these, the 6-fold coordination of Mg^{2+} is achieved in a way similar to that of the 7-fold coordination of Ca^{2+} *(23−25)*. In the crystal structure of $(Mg^{2+})_1$−calbindin D_{9k} *(25)*, Mg^{2+} is coordinated by the same ligands as Ca^{2+} with the exception of a water molecule replacing a glutamic acid. The bidentate Ca^{2+} ligation by the side chain carboxylate oxygens of this glutamic acid has been found crucial for the Ca^{2+}-induced structural rearrangements *(26−29)*. A recent NMR study of the N-terminal domain *(30)* suggests that Mg^{2+} binds to the same sites as Ca^{2+} with binding constants in the millimolar range, implying that the domain is saturated to almost 50% by Mg^{2+} at resting Ca^{2+} levels. No structure of Mg^{2+}-loaded CaM is available, but the NMR data suggest a coordination

[†] This research was supported by grants from the Swedish Natural Science Research Council to S.L., S.F., and T.D. The 600 MHz spectrometer was purchased by a grant from the Knut and Alice Wallenberg Foundation.

* Corresponding author. Fax: +1-858-784-9985. E-mail: anders@scripps.edu.

[‡] Present address: Department of Molecular Biology, MB-9, The Scripps Research Institute, 10550 North Torrey Pines Rd., La Jolla, CA 92037.

[1] Abbreviations: 5N-BAPTA, 5-nitro-1,2-bis(2-aminophenoxy)-ethane-*N*,*N*,*N*′,*N*′-tetraacetic acid; CaM, calmodulin; TR_1C, the recombinant N-terminal domain of calmodulin (Ala1−Asp80) with an additional N-terminal Met; TR_2C, the recombinant C-terminal domain of calmodulin (Met76−Lys148).

10.1021/bi9909288 CCC: $18.00
Published on Web 08/17/1999

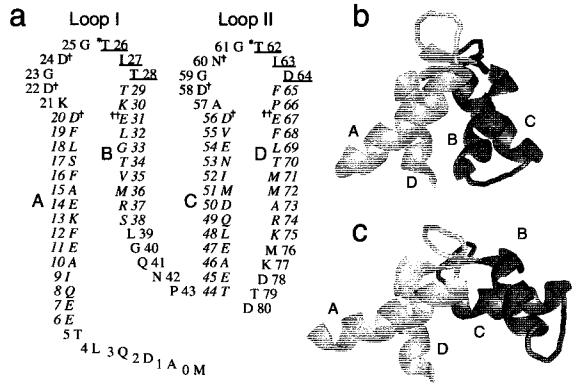

FIGURE 1: Amino acid sequence and secondary structure (a) and three-dimensional structures of the "closed" ion-free *(53)* (b) and "open" Ca^{2+}-loaded *(54)* (c) states of the N-terminal domain of CaM (TR_1C). In (a) the one letter code for amino acid residues is used. The secondary structure of TR_1C *(53)* is indicated with *helical* residues in *italics* and *β-sheet* residues *underlined*. The Ca^{2+} coordination is indicated as follows: mainchain carbonyl oxygens, asterisk (*); monodentate carboxylates, dagger (†); bidentate carboxylates, double daggers (††). The helices are denoted A−D. In (b) and (c) residues Thr5−Ile27 and Ile63−Lys75 are colored light gray and Thr28−Thr62 are dark gray. The *β*-strands (Thr26−Thr28, Thr62−Asp64) are oriented similarly in the two structures. This figure was generated using UCSF software Midas Plus *(55)*.

similar to that revealed in $(Mg^{2+})_1$−calbindin D_{9k}. This offers an explanation to why Mg^{2+} does not trigger the major structural rearrangements that occur upon Ca^{2+} binding *(30* and references therein*)*. Consequently, targets proteins are negligibly activated by Mg^{2+}-loaded CaM *(31, 32)*.

The goal of the present work is to understand the role of Mg^{2+} in Ca^{2+}/CaM signaling at physiological conditions. The Ca^{2+} affinity of the TR_1C fragment of vertebrate CaM (comprising residues Ala1−Asp80 and an additional N-terminal Met) was measured as a function of Mg^{2+} concentration, using a fluorescent chelator. In addition, the Ca^{2+} and protein equilibria and kinetics as a function of Mg^{2+} concentration were monitored in Mg^{2+}−Ca^{2+} competition studies using ^{43}Ca NMR and ^{1}H−^{15}N NMR.

MATERIALS AND METHODS

Protein Synthesis. The synthetic gene for TR_1C was constructed from a cloned CaM gene by PCR, using oligonucleotide primers to yield the TR_1C gene flanked by cloning sites for the expression vector. The gene was cloned into the pRCB1 plasmid. Unlabeled and uniformly ^{15}N-labeled TR_1C was expressed in *Escherichia coli* and purified as reported previously for the TR_2C fragment *(20)*.

Chelator Method. The macroscopic Ca^{2+}-binding constants were determined as described by Linse et al. *(22)*, using the fluorescent Ca^{2+} chelator 5N-BAPTA *(33)*. The absorbance at 430 nm was measured as $CaCl_2$ was added up to a final concentration of 2.5 mM, in solutions containing 0.028 mM 5N-BAPTA and 0.074 mM TR_1C or 0.030 mM 5N-BAPTA and 0.024 mM TR_1C in 2.0 mM TRIS/HCl buffer at 25 °C, pH 7.5, 150 mM KCl, and 0, 0.4, 2.0, and 10 mM $MgCl_2$, respectively. The chelator 5N-BAPTA was chosen because of a Ca^{2+} affinity in the appropriate range and high level of discrimination against Mg^{2+} (log $K_{Ca} = 4.61$, 4.57, and 4.46 in 150 mM KCl and 0, 2, and 10 mM $MgCl_2$, respectively). The protein concentration was determined by amino acid analysis after acid hydrolysis.

^{43}Ca NMR. The line width of the ^{43}Ca NMR signal was followed when $MgCl_2$ was added, 0−180 mM, to a solution of 0.35 mM $^{43}CaCl_2$ and 0.18 mM TR_1C in 100 mM KCl at pH 7.2, 25 °C, in a 5 mL egg-shaped sample tube. In addition, the line width of the ^{43}Ca signal was followed as the temperature was varied between 5 and 45 °C for a solution of 0.39 mM $^{43}CaCl_2$ and 0.21 mM TR_1C in 100 mM KCl and 0 or 23 mM $MgCl_2$, respectively, at pH 7.2. At each titration point, pH was adjusted to 7.2 by microliter additions of 0.1 M HCl or KOH. The final protein, Mg^{2+}, and Ca^{2+} concentrations were determined by amino acid analysis after acid hydrolysis and atomic absorption spectrophotometry, respectively. The ^{43}Ca NMR spectra were obtained at 24.2 MHz using an Oxford Instrument 360 WB magnet operating at a ^{1}H frequency of 360 MHz equipped with a horizontal solenoid probe *(34)* and interfaced with a Varian Unity 400 console. A 90° pulse width of 35 μs and a spectral width of 10 kHz was used throughout these measurements. The RIDE *(35)* pulse sequence was used to reduce effects of probe ringing. Line widths were determined using the VNMR program.

The theoretical line shape can be obtained by solving the Bloch−McConnell equations *(36)* for exchange between N sites.

$$\frac{d\mathbf{M}_j^+(t)}{dt} = i\delta_j\omega_0\mathbf{M}_j^+(t) - R_{2j}^0\mathbf{M}_j^+(t) + \sum_{k=1}^{N} k_{jk}\mathbf{M}_k^+(t) \quad (1)$$

where $\mathbf{M}_j^+$ is the transverse magnetization matrix at site state j, δ_j is the chemical shift at site j, $\omega_0 = 24.2$ MHz is the ^{43}Ca frequency, R_{2j}^0 is the exchange-free transverse relaxation rate at site j, and k_{jk} is the transition rate from site k to site j. In the extreme narrowing regime ($\omega_0\tau_c \ll 1$) valid for free Ca^{2+},

$$R_{2j}^0 = \frac{3\pi^2\chi_j^2(2I+3)\tau_{cj}}{10[I^2(2I+1)]} \quad (2)$$

where χ_j is the nuclear quadrupole coupling constant proportional to the electric field gradient, which is assumed to be symmetric, $I = {}^7/_2$ is the spin of ^{43}Ca, and τ_{cj} is the rotational correlation time. For a free Ca^{2+} $\tau_c \sim 10$ ps and the resulting line width can be neglected. In the near extreme narrowing regime ($\omega_0\tau_c < 1.5$, but not small compared to unity), valid for bound Ca^{2+}, which tumbles with the protein *(37−39)*,

$$R_{2j}^0 = \frac{3\pi^2\chi_j^2(2I+3)}{100[I^2(2I+1)]}\left(3\tau_{cj} + \frac{5\tau_{cj}}{1+(\omega_0\tau_{cj})^2} + \frac{2\tau_{cj}}{1+(2\omega_0\tau_{cj})^2}\right) \quad (3)$$

For TR_1C at 25 °C $\tau_c \approx 4$ ns. The transition rate from site k to state j is assumed to obey transition state theory.

$$k_{jk} = \frac{kT}{h}e^{-(\Delta H^{\ddagger}_{jk} - T\Delta S^{\ddagger}_{jk})/RT} \quad (4)$$

where $\Delta H^{\ddagger}_{jk}$ and $\Delta S^{\ddagger}_{jk}$ are the transition enthalpy and entropy, respectively, k is Boltzmann's constant, h is Plank's constant, R is the gas constant, and T is the absolute temperature.

The rotational correlation time is assumed to be temperature dependent

$$\frac{1}{\tau_{cj}} = \frac{kT}{h} e^{-\Delta G_{0j}/RT} \quad (5)$$

where ΔG_{0j} is the activation free energy of rotation.

A program using eqs 1−5 to calculate line shapes for chemical exchange between up to four sites was used. Line widths of experimental or calculated signals are given as the full width at half-height of the Lorentzian line yielding the best fit *(2, 40, 41)*.

$^1H-^{15}N$ NMR. Chemical shifts and line widths of ^1H and ^{15}N resonances were followed in a Mg^{2+} titration of Ca^{2+}-saturated TR_1C at 25 °C, pH 7.5, on a 0.15 mM ^{15}N-labeled TR_1C sample in H_2O with 10% D_2O, 0.75 mM $CaCl_2$, 150 mM KCl, 100 μM NaN_3, and 10 μM DSS. Aliquots of Mg^{2+} were added as solutions of $MgCl_2$. The resulting Mg^{2+} concentrations were 0, 0.3, 0.7, 1.2, 2.7, 5.8, 11, 18, 35, and 66 mM. The final protein and the Mg^{2+} and Ca^{2+} concentrations were determined by amino acid analysis after acid hydrolysis and atomic absorption spectrophotometry, respectively. At each titration point, pH was adjusted to 7.5 by microliter additions of 0.1 M HCl or KOH. The $^1H-^{15}N$ NMR spectra were recorded on a Varian Unity Plus spectrometer at a ^1H frequency of 599.89 MHz. Sensitivity-enhanced and gradient-selected 2D $^1H-^{15}N$ HSQC NMR spectra *(42)* were recorded with spectral widths of 1600 and 7692 Hz, sampled over 256 and 2048 complex data points in the ^{15}N- and ^1H-dimension, respectively. Using 18 scans per t_1 increment and a relaxation delay of 1.5 s between scans, the total experimental time was 3.5 h per spectrum. ^{15}N-nuclei were decoupled during acquisition using the GARP-1 sequence *(43)*. ^1H chemical shifts were referenced to DSS at 0 ppm, and ^{15}N-chemical shifts indirectly via the ^1H frequency using the frequency ratio ($^{15}N/^1H$) of 0.101 329 118 *(44)*. The spectra were processed using a Lorentzian line broadening window function in ω_2 and a 60° shifted sine-squared window function in ω_1. After zero-filling in ω_1 the matrix size was 1024 × 512 real points. The line widths were determined using the in-house curve fitting software CFIT (Gippert, G. P., unpublished material) as described previously *(30)*.

Data Evaluation. Binding data were evaluated under the assumption that both Ca^{2+} and Mg^{2+} can bind to the same two sites, as shown in Figure 2a. In total five macroscopic binding constants, shown in Figure 2b, are necessary to describe the equilibria between the different ion-bound states and the apo state:

$$p_{Ca1} = K_{Ca1}[Ca^{2+}]p_{Apo} \quad (6)$$

$$p_{Ca2} = K_{Ca2}[Ca^{2+}]p_{Ca1} \quad (7)$$

$$p_{Mg1} = K_{Mg}[Mg^{2+}]p_{Apo} \quad (8)$$

$$p_{Mg2} = K_{Mg2}[Mg^{2+}]p_{Mg1} \quad (9)$$

$$p_{MgCa} = K_{MgCa}[Mg^{2+}][Ca^{2+}]p_{Apo} \quad (10)$$

where p_{Apo}, p_{Ca1}, p_{Ca2}, p_{Mg1}, p_{Mg2}, and p_{MgCa} are the populations of the apo, $(Ca^{2+})_1$, $(Ca^{2+})_2$, $(Mg^{2+})_1$, $(Mg^{2+})_2$ and $(Mg^{2+})_1(Ca^{2+})_1$ state, respectively, and K_i are the macroscopic binding constants. Notice that the macroscopic treatment makes no distinction between different forms containing the same combination of ions. Since the measurements were performed in the presence of 100 and 150 mM KCl, unspecific effects of Mg^{2+} due to increased ionic strength were neglected.

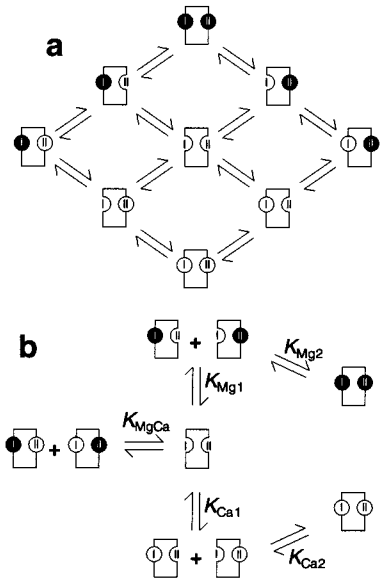

FIGURE 2: (a) Model of the equilibria of Ca^{2+} and Mg^{2+} binding to TR_1C and (b) macroscopic binding constants describing Ca^{2+} (open circles) and Mg^{2+} (filled circles) binding.

Table 1: Ca^{2+} Binding Constants of TR_1C[a]

solution conditions	log $K_{Ca1}K_{Ca2}$
150 mM KCl	9.7 ± 0.1
150 mM KCl, 0.4 mM Mg^{2+}	9.4 ± 0.1
150 mM KCL, 2 mM Mg^{2+}	9.0 ± 0.08
150 mM KCl, 10 mM Mg^{2+}	8.0 ± 0.08

[a] The apparent binding constants for two Ca^{2+}, $K_{Ca1}K_{Ca2}$ (reported as log $K_{Ca1}K_{Ca2}$), derived from metal ion titrations using a Ca^{2+} chelator.

RESULTS

Chelator Method. The apparent Ca^{2+}-binding constants at 0, 0.4, 2, and 10 mM $MgCl_2$, respectively, were measured using the fluorescent Ca^{2+} chelator 5N-BAPTA and at high ionic strength (150 mM KCl), as displayed in Table 1. Only the value of $K_{Ca1}K_{Ca2}$ is reported since Ca^{2+} binding is too cooperative to reliably resolve the individual binding constants. To check the validity of the assumption of competitive binding, the mean value of the Mg^{2+} binding constant, $K_{Mg,mean}$, was estimated from $K_{Ca,mean,app} = [(K_{Ca1}K_{Ca2})_{app}]^{1/2}$ at each Mg^{2+} concentration, using an equation describing the competition of two ions for a single site *(45)* (Figure 3).

$$K_{Ca,mean,app} = \frac{K_{Ca,mean}}{1 + K_{Mg,mean}[Mg^{2+}]} \quad (11)$$

where $K_{Ca,mean} = (K_{Ca1}K_{Ca2})^{1/2}$ is the value obtained in the absence of Mg^{2+}. The estimated log $K_{Mg,mean} = 2.74 \pm 0.05$ agrees with log $K_{Mg,mean} = 2.88 \pm 0.12$ obtained from the

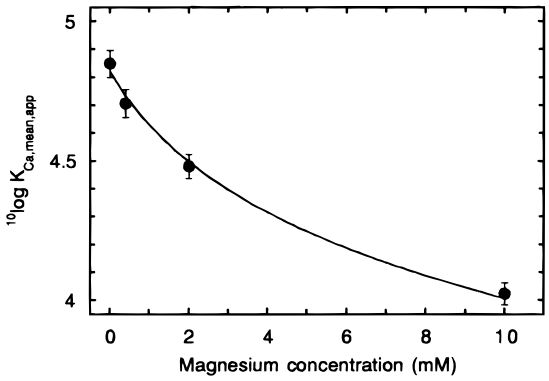

FIGURE 3: Logarithmic mean calcium binding constants as a function of $MgCl_2$ concentration. The line was fitted using eq 11. Uncertainties were estimated as the deviation from the optimized value causing a doubling of the error square sum.

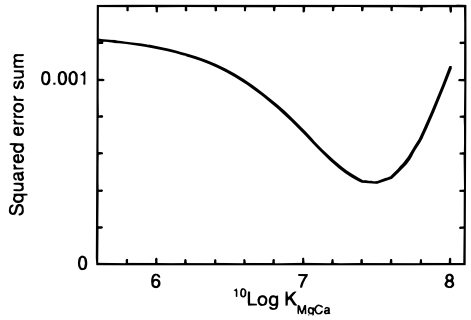

FIGURE 4: Total error square sum as a function of log K_{MgCa} for the 2 chelator titrations at 10 mM Mg^{2+}.

previously determined microscopic binding constants *(30)* and implies a reduction of $K_{Ca,mean,app}$ by about a factor of 1.6 at physiological Mg^{2+} levels.

The mixed ion binding constant, K_{MgCa}, was optimized against chelator data and previously determined binding constants *(22, 30)* which were allowed to vary within their error limits. K_{MgCa} is not very well determined from these measurements. However, log $K_{MgCa} = 7.4 \pm 0.5$ could be estimated from the data obtained in 10 mM $MgCl_2$ (Figure 4).

^{43}Ca NMR. The line width of the ^{43}Ca signal in the presence of TR_1C decreases as Mg^{2+} is added, as shown in Figure 5a. This suggests that Ca^{2+} is displaced by Mg^{2+} since they compete for the same binding sites. When the Ca^{2+} exchange is fast on the ^{43}Ca NMR time scale (>2000 s^{-1}), the ^{43}Ca line width is calculated as

$$\Delta\nu_{1/2} = p_f\Delta\nu_f + p_b\Delta\nu_b \qquad (12)$$

where $\Delta\nu_f$ and $\Delta\nu_b$ are the line widths of the resonance of free and bound ^{43}Ca, respectively, and p_f and p_b are their respective populations (Figure 5a). The Mg^{2+} affinity calculated using this relation was log $K_{Mg,mean} = 3.7$, a value that is significantly higher than those previously obtained *(30)*.

Under conditions of intermediate exchange, the interpretation is much more complex because the signals are non-Lorentzian, even though the deviation from a Lorentzian line shape associated with this effect could not be observed at the signal-to-noise level of the present study. To determine the exchange conditions the temperature dependence of the ^{43}Ca line width was measured in the presence of 0 and 20 mM Mg^{2+} (Figure 6). Using eqs 1−5 it can be shown that the Ca^{2+} off-rate increases at increasing Mg^{2+} concentrations.

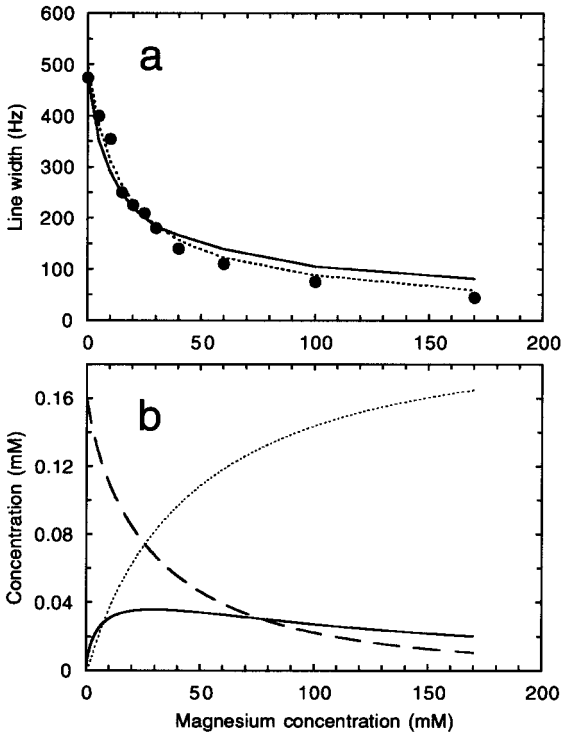

FIGURE 5: (a) ^{43}Ca line width at 25 °C, pH 7.2, in 100 mM KCl as a function of $MgCl_2$ concentration (filled circles). The solid line was calculated using $k_{off} = 6600\ s^{-1}$ for the $(Mg^{2+})_1(Ca^{2+})_1$ state and the parameters in Table 2, and the dotted line was calculated with the assumption of one fast exchanging site. (b) Concentrations of the $(Mg^{2+})_1(Ca^{2+})_1$ state (solid line), $(Ca^{2+})_2$ state (dashed line), and $(Mg^{2+})_2$ state (dotted line) as a function of Mg^{2+} concentration, calculated using the parameters in Table 2.

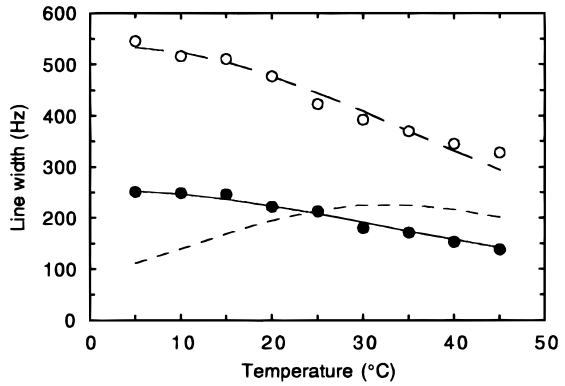

FIGURE 6: ^{43}Ca line width as a function of temperature in the absence (open circles) and presence (filled circles) of 20 mM Mg^{2+} at 25 °C, pH 7.2, in 100 mM KCl. The upper dashed curve shows the line width calculated using the activation parameters reported previously *(46)*. The lower dashed curve has been calculated with the same parameters with the population of free Ca^{2+} adjusted to obtain the proper line width at 25 °C. The best agreement with experimental line widths is shown by the solid curve obtained using a quadrupolar coupling that is 20% larger than in the $(Ca^{2+})_2$ state ($\chi = 1.22$ MHz) and an off-rate of 6600 s^{-1} (compared to 500 s^{-1} at 25 °C for the upper curve).

The upper dashed curve represents the calculated ^{43}Ca NMR line width as a function of temperature in the absence of Mg^{2+}, using the activation parameters reported previously ($\Delta G^{\ddagger} = 58$ kJ/mol) *(46)*, resulting in an off-rate of 500 s^{-1} at 25 °C. The lower dashed curve, calculated using the same activation parameters but with the population of free Ca^{2+} adjusted to obtain the proper line width at 25 °C in the

Table 2: Macroscopic Binding Constants

binding constant	log K	binding constant	log K
K_{Ca1}[a]	4.0 ± 0.3	K_{Mg1}[b]	3.2 ± 0.2
$K_{Ca1}K_{Ca2}$	9.7 ± 0.1	$K_{Mg1}K_{Mg2}$[b]	5.8 ± 0.4
K_{MgCa}	7.6 ± 0.3		

[a] Obtained from Linse et al. *(22)*. [b] Obtained from Malmendal et al. *(30)*.

presence of 20 mM Mg^{2+}, shows that these parameters are incompatible with the data obtained in 20 mM Mg^{2+}. One probable explanation is that the dominating Ca^{2+}-containing species at these conditions is the $(Mg^{2+})_1(Ca^{2+})_1$ state with a fast Ca^{2+} off-rate. This means that three Ca^{2+} states should be considered under the experimental conditions: Ca^{2+} bound to the $(Mg^{2+})_1(Ca^{2+})_1$ state; Ca^{2+} bound to the $(Ca^{2+})_2$ state; free Ca^{2+}. Assuming that the binding constants are independent of temperature, we can estimate a lower limit of log $K_{MgCa} = 7.3$ below which the population of the $(Mg^{2+})_1(Ca^{2+})_1$ state is too low to account for the observed temperature dependence of the ^{43}Ca signal. Thus, the range of allowed values obtained from the chelator measurements is reduced to log $K_{MgCa} = 7.6 \pm 0.3$, indicating a slightly positive allosteric interaction of ~2 kJ/mol. Populations of all species present during the ^{43}Ca NMR experiment can be calculated from the binding constants in Table 2 as shown in Figure 5b. If log $K_{MgCa} = 7.6$ is used, only two adjustable parameters remain in eqs 1−5, the quadrupolar coupling constant χ for ^{43}Ca in the $(Mg^{2+})_1(Ca^{2+})_1$ state and the off-rate of Ca^{2+} from this state. The best agreement with experimental line widths, as shown by the solid curve in Figure 6, is obtained using a quadrupolar coupling constant that is 20% larger than in the $(Ca^{2+})_2$ state ($\chi = 1.22 \pm 0.05$ MHz) and an off-rate of 6600 ± 500 s^{-1} ($\Delta G^{\ddagger} = 51.1$ kJ/mol), compared to 500 s^{-1} for the $(Ca^{2+})_2$ state at 25 °C. The off-rate of Ca^{2+} bound to TR_1C in the presence of 20 mM Mg^{2+} have thus increased about 10-fold as compared to the value in the absence of Mg^{2+}. Using the same constants, the line width at 25 °C depends on the Mg^{2+} concentration as shown by the solid curve in Figure 5a.

$^1H-^{15}N$ NMR. ^1H and ^{15}N chemical shifts and ^1H line widths of backbone and side chain $^1H-^{15}N$ pairs were determined from HSQC spectra of 0.15 mM TR_1C as a function of the Mg^{2+} concentration (0−66 mM), in the presence of 0.75 mM $CaCl_2$ and 150 mM KCl. The starting conditions were such that the protein was 99% Ca^{2+}-saturated. As Mg^{2+} was added most signals were broadened. Some signals show line width maxima around 20 mM Mg^{2+}, while others are continuously broadened throughout the titration. The chemical shift and line width curves can be reasonably well accounted for by an exchange from the $(Ca^{2+})_2$ state via a $(Mg^{2+})_1(Ca^{2+})_1$ state to the $(Mg^{2+})_2$ state with the binding constants and exchange rates discussed above.

The chemical shifts of the $(Mg^{2+})_1(Ca^{2+})_1$ state, δ_{MgCa}, were determined under the assumption of chemical exchange, k_{ex}, that is fast on the chemical shift time scale ($k_{ex} \gg 2\pi\nu_0\Delta\delta$, where ν_0 is the spectrometer frequency for the nucleus in MHz and $\Delta\delta$ is the chemical shift difference between the two states in ppm).

$$\delta_{MgCa} = \frac{\delta_{obs} - p_{Ca2}\delta_{Ca2} - p_{Mg2}\delta_{Mg2}}{p_{MgCa}} \qquad (13)$$

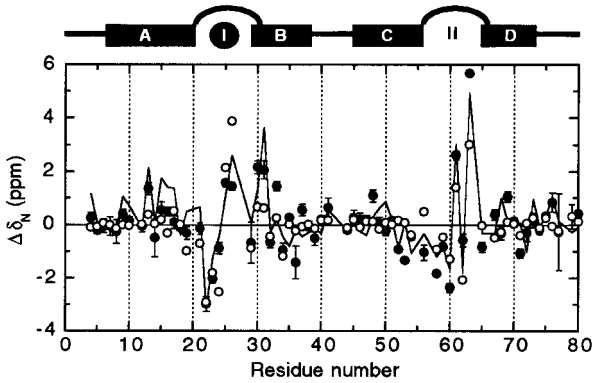

FIGURE 7: Backbone amide ^{15}N chemical shift changes induced by binding of one Mg^{2+} and one Ca^{2+} (filled circles), two Ca^{2+} (line), and two Mg^{2+} (open circles). The chemical shifts of the apo and pure Ca^{2+} and Mg^{2+} states were obtained from ref *30*. The dark rectangles represent α-helical regions, and arcs represent loop regions.

where δ_{obs} is the measured chemical shift, δ_{Ca2} and δ_{Mg2} are the chemical shifts of the fully Ca^{2+} and Mg^{2+} saturated states, respectively, determined previously *(30)*, and p_{Ca2}, p_{Mg2}, and p_{MgCa} are the populations of the three fully saturated states. Because of the high Ca^{2+} levels, the populations of the apo and half-saturated states could, to a good approximation, be neglected.

The chemical shifts of the $(Mg^{2+})_1(Ca^{2+})_1$ state are difficult to determine accurately. This state has a limited population (maximum 25%), and the exchange rates with the $(Ca^{2+})_2$- and $(Mg^{2+})_2$ states are not very fast on the chemical shift time scale *(47)*. Thus, large differences between δ_{Ca2} and δ_{MgCa} will be underestimated since the true weight of the δ_{MgCa} in the observed chemical shift will be smaller than the weight calculated from the populations. To minimize such errors, δ_{MgCa} was not calculated for nuclei with differences between δ_{Ca2} and δ_{Mg2} larger than 200 Hz (0.33 and 3.3 ppm for ^1H and ^{15}N, respectively). To limit the weight of small deviations in δ_{Mg2} compared to previously determined values *(30)*, only chemical shifts at Mg^{2+} concentrations less than 10 mM were included in the fit. The obtained backbone ^{15}N shifts are shown in Figure 7.

DISCUSSION

The equilibria evaluated above include two types of ions and a protein with two interacting ion-binding sites (Figure 2a). Each site can be either empty or have one of the two ions bound. The interaction between the site and a given ion may depend on what is bound to the other site, implying that each site can have three different binding kinetics and equilibria for each ion. To define these interactions, three different methods were used. The chelator method measures the ratio between free and total calcium at low protein concentrations. The competition for the ions between the protein sites and the chelator enables measurements of the macroscopic binding constants for proteins that bind Ca^{2+} cooperatively. However, even this method has a limited capability to resolve the individual binding constants above a certain degree of cooperativity. The signal line width in ^{43}Ca NMR is dependent on the exchange rates and equilibria between different environments for Ca^{2+}. Similarly the chemical shifts and line widths in $^1H-^{15}N$ NMR depend on the exchange rates and equilibria between different states of

the protein. Many of the exchange processes occur on intermediate ^{1}H and ^{15}N NMR time scales, resulting in broadened resonances and/or signal loss. The NMR methods need significantly higher protein concentrations than the chelator method, and as a consequence, much higher ion concentrations are used.

Ca^{2+}−Mg^{2+} Binding. The data presented in this work clearly show that Mg^{2+} and Ca^{2+} compete for the same sites in TR_1C. This does not exclude the presence of auxiliary binding sites, but the data are obviously not compatible with the conclusion of Gilli et al. *(5)* that Mg^{2+} does not compete with Ca^{2+} for the EF-hand sites. In the three available three-dimensional structures of Mg^{2+} bound to EF-hand proteins *(23*−*25)* Mg^{2+} is bound in the EF-hand site with no possibility of simultaneous Mg^{2+} and Ca^{2+} coordination in the same site.

The slightly positive allosteric interaction between Mg^{2+} and Ca^{2+} binding is different from the significantly negative allosteric Ca^{2+}−Mg^{2+} interaction which was recently found in calbindin D_{9k} *(25)*. Even if the two proteins share many features, the rigid and Ca^{2+}-selective N-terminal *pseudo* EF-hand of calbindin D_{9k} and its different responses to Ca^{2+} and Mg^{2+} binding may well explain the difference *(25)*.

Ca^{2+} Off-Rate. The Ca^{2+} off-rate of 6600 s^{-1} from the $(Mg^{2+})_1(Ca^{2+})_1$ state is significantly faster than the off-rate of 500 s^{-1} measured for the $(Ca^{2+})_2$ state. On the other hand, the much faster off-rate agrees well with that the allosteric interaction with Mg^{2+} is much lower than the cooperative interaction with an other Ca^{2+}. Assuming that the Ca^{2+} on-rate is diffusion-limited for all species (5×10^8 s^{-1} M^{-1}), we can estimate the off-rates from the knowledge of the binding constants; however, this relies on the possibility to resolve the binding constants K_{Ca1} and K_{Ca2} and not only the product $K_{Ca1}K_{Ca2}$. The value of log $K_{Ca1} = 4$ would give a k_{off} from the $(Ca^{2+})_1$ state of 50 000 s^{-1} and a value 1000 s^{-1} for the $(Ca^{2+})_2$ state. This latter value agrees reasonably well with the previously determined value of 500 s^{-1}. Similarly the exchange rate of Ca^{2+} from the $(Mg^{2+})_1(Ca^{2+})_1$ state may be estimated from log $K_{MgCa} = 7.6$ and log $K_{Mg1} = 3.2$ to be approximately 20 000 s^{-1}, which should be compared to our estimated Ca^{2+} off-rate from the $(Mg^{2+})_1$-$(Ca^{2+})_1$ state, of 6600 s^{-1}, a reasonable agreement considering all assumptions made. An off-rate of about 10 000 s^{-1} was estimated for Mg^{2+} from loop II *(30)*. In a recent study of the TR_2C fragment the Ca^{2+} off-rate from its $(Ca^{2+})_1$ state was estimated to be about 15 000 s^{-1} *(48)*.

Structure of the $(Mg^{2+})_1(Ca^{2+})_1$ State. The faster Ca^{2+} off-rate from the $(Mg^{2+})_1(Ca^{2+})_1$ state indicates that this state is structurally and/or dynamically different from the $(Ca^{2+})_2$ state. The calculated backbone ^{15}N chemical shifts of the $(Mg^{2+})_1(Ca^{2+})_1$ state shown in Figure 7 should be interpreted with caution because of the fragility of the calculations. However, the chemical shifts of helix A, which are very similar to those of the apo and $(Mg^{2+})_2$ states and not to the $(Ca^{2+})_2$ state, indicate a closed conformation of the N-terminal EF-hand. Even though the chemical shifts of the rest of the protein are hard to interpret, they may well agree with the accommodation of the ions in an essentially closed structure. The 20% larger ^{43}Ca quadrupolar coupling constant compared to the $(Ca^{2+})_2$ state ($\chi = 1.22 \pm 0.05$ MHz) indicates a lower symmetry in the coordination sphere *(49)* which may be interpreted as usage of different ligands. One explanation may be that the bidentate glutamic acid in the 12th loop position does not coordinate Ca^{2+} in this state, which further points toward a closed structure.

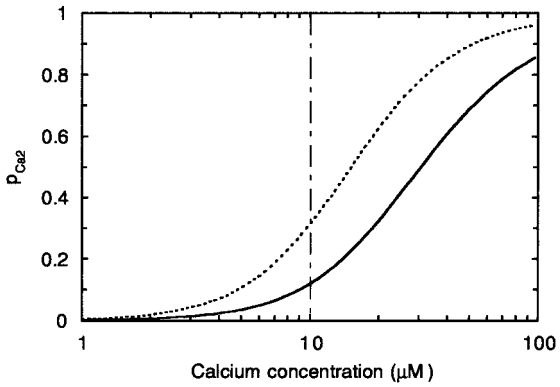

FIGURE 8: Population of the Ca^{2+}-loaded state of TR_1C as a function of free Ca^{2+} in the presence (solid line) and absence (dotted line) of 1 mM Mg^{2+} calculated using the parameters in Table 2. The dash−dotted line represents the upper limit for the intracellular Ca^{2+} concentration.

Ion Selectivity of EF-Hand Loops. It has earlier been shown that loop I has the highest affinity for Mg^{2+} *(4, 30)*. In a study of a 33 residue EF-hand helix−loop−helix construct, a loop sequence where the residues in positions three, five, and nine were the same as in loop I, except for a Ser instead of a Thr in position nine (Figure 1a), had higher Mg^{2+} affinity and slightly lower Ca^{2+} affinity than with the same residues as in loop II in these positions *(50)*. This is in agreement with the calculated $(Mg^{2+})_1(Ca^{2+})_1$ chemical shifts for helix A which are very similar to those of the $(Mg^{2+})_2$ state, suggesting that it is mainly loop I that harbors Mg^{2+}. A difference in Ca^{2+} affinity between the loops is also suggested by equilibrium titration measurements on intact CaM, showing about 5-fold stronger Ca^{2+} binding to one of the loops in the N-terminal domain *(51)*. In the C-terminal domain of CaM a higher Ca^{2+} affinity of the C-terminal loop IV is indicated by both binding constants of binding-site mutants *(26, 29)*, and the chemical shifts of the $(Ca^{2+})_1$ state as monitored by ^{15}N-relaxation measurements *(48)*.

Physiological Implications of Mg^{2+}−Ca^{2+} Interference. The competition of the about 1 mM Mg^{2+} present in the cytosol for the same sites as Ca^{2+} has significant effects on the population of the activated Ca^{2+}-loaded state of the N-terminal domain of CaM. Even if $K_{Ca,mean,app}$ is reduced by only a factor of 1.6, the population of the Ca^{2+}-loaded state is about a factor of 2.6−3.3 lower in the presence of Mg^{2+} in the entire range of cytosolic Ca^{2+} concentrations (Figure 8). This imply that no more than 10% of the N-terminal domains of the CaM molecules that are not complexed with a target protein are ever fully Ca^{2+}-loaded. When CaM binds to a target molecule in a Ca^{2+}-dependent way, the apparent Ca^{2+}-affinity is significantly increased *(52)*. It is therefore highly plausible that Ca^{2+} generally does not bind to the N-terminal domain until binding to the target and that this event is triggered by Ca^{2+} binding to the higher affinity C-terminal domain. A significant decrease in the affinity for target molecules in the presence of Mg^{2+} has been observed *(4)*. Furthermore, the rate of Ca^{2+} binding to the N-terminal domain is likely to be limited by the Mg^{2+} off-rate. Following the same line of reasoning as for the Ca^{2+} off-rate, i.e., that the on-rate is constant, an off-rate of the

order of 100 s^{-1} is estimated for loop I. The Ca^{2+} on-rate would be rate-limiting only if the presence of a Ca^{2+} ion in loop II speeds up the Mg^{2+} dissociation from loop I by a factor of at least 100.

CONCLUSIONS

Mg^{2+} and Ca^{2+} binding data are well described by a two-site model in which each site can bind either Ca^{2+} or Mg^{2+} but not both ions simultaneously. The apparent affinity for Ca^{2+} is significantly decreased at physiological Mg^{2+} levels, so that at Ca^{2+} concentrations of an activated cell the $(Ca^{2+})_2$ state of this domain is only weakly populated. This suggests that for this domain Ca^{2+} binding is intimately associated with target binding. The faster Ca^{2+} off-rate from the $(Mg^{2+})_1(Ca^{2+})_1$ state and the slightly positive allosteric $Mg^{2+}-Ca^{2+}$ binding interaction indicate that the structure of this state is different from the $(Ca^{2+})_2$ state. This is also suggested by the ^{43}Ca quadrupolar coupling constant and the ^{1}H and ^{15}N chemical shifts of the $(Mg^{2+})_1(Ca^{2+})_1$ state calculated from titration data, which are both suggestive of a conformation more similar to the "closed" apo and $(Mg^{2+})_2$ states than to the "open" $(Ca^{2+})_2$ state.

ACKNOWLEDGMENT

We thank Eva Thulin for protein expression and purification.

REFERENCES

1. Ogawa, Y., and Tanokura, M. (1984) *J. Biochem. 95*, 19−28.
2. Tsai, M.-D., Drakenberg, T., Thulin, E., and Forsén, S. (1987) *Biochemistry 26*, 3635−3643.
3. Lafitte, D., Capony, J. P., Grassy, G., Haiech, J., and Calas, B. (1995) *Biochemistry 34*, 13825−13832.
4. Ohki, S.-y., Ikura, M., and Zhang, M. (1997) *Biochemistry 36*, 4309−4316.
5. Gilli, R., Lafitte, D., Lopez, C., Kilhoffer, M.-C., Makarov, A., Briand, C., and Haiech, J. (1998) *Biochemistry 37*, 5450−5456.
6. Berridge, M. J., Bootman, M. D., and Lipp, P. (1998) *Nature 395*, 645−648.
7. Evenäs, J., Malmendal, A., and Forsén, S. (1998) *Curr. Opin. Chem. Biol. 2*, 293−302.
8. Ebel, H., and Gunther, T. (1980) *J. Clin. Chem. Clin. Biochem. 18*, 257−270.
9. Needham, J. V., Chen, T., and Falke, J. J. (1993) *Biochemistry 32*, 3363−3367.
10. Falke, J. J., Drake, S. K., Hazard, A. L., and Peersen, O. B. (1994) *Q. Rev. Biophys. 27*, 219−290.
11. Linse, S., and Forsén, S. (1995) in *Calcium Regulation of Cellular Function* (Means, A. R., Ed.) pp 89−152, Raven Press, New York.
12. Kretsinger, R. H., and Nockolds, C. B. (1973) *J. Biol. Chem. 248*, 3313−3326.
13. Klee, C. B. (1988) in *Calmodulin* (Cohen, P., and Klee, C. B., Eds.) pp 35−56, Elsevier, New York.
14. Crivici, A., and Ikura, M. (1995) *Annu. Rev. Biophys. Biomol. Struct. 24*, 85−116.
15. Finn, B. E., and Forsén, S. (1995) *Structure 3*, 7−11.
16. Celio, M. R., Pauls, T., and Schwaller, B. (1996) *Guidebook to the calcium-binding proteins*, 1st ed., Oxford University Press, Oxford, U.K.
17. Drabikowski, W., Kuznicki, J., and Grabarek, Z. (1977) *Biochim. Biophys. Acta 485*, 124−133.
18. Walsh, M., Stevens, F. C., Kuznicki, J., and Drabikowski, W. (1977) *J. Biol. Chem. 252*, 7440−7443.
19. Finn, B. E., Drakenberg, T., and Forsén, S. (1993) *FEBS Lett. 336*, 368−374.
20. Finn, B. E., Evenäs, J., Drakenberg, T., Waltho, J. P., Thulin, E., and Forsén, S. (1995) *Nat. Struct. Biol. 2*, 777−783.
21. Bentrop, D., Bertini, I., Cremonini, M. A., Forsén, S., Luchinat, C., and Malmendal, A. (1997) *Biochemistry 36*, 11605−11618.
22. Linse, S., Helmersson, A., and Forsén, S. (1991) *J. Biol. Chem. 266*, 8050−8054.
23. Declercq, J. P., Tinant, B., Parello, J., and Rambaud, J. (1991) *J. Mol. Biol. 220*, 1017−1039.
24. Houdusse, A., and Cohen, C. (1996) *Structure 4*, 21−32.
25. Andersson, M., Malmendal, A., Linse, S., Ivarsson, I., Forsén, S., and Svensson, L. A. (1997) *Protein Sci. 6*, 1139−1147.
26. Evenäs, J., Thulin, E., Malmendal, A., Forsén, S., and Carlström, G. (1997) *Biochemistry 36*, 3448−3457.
27. Gagné, S. M., Li, M. X., and Sykes, B. D. (1997) *Biochemistry 36*, 4386-4392.
28. Li, M. X., Gagné, S. M., Spyracopoulos, L., Kloks, C. P. A. M., Audette, G., Chandra, M., Solaro, R. J., Smillie, L. B., and Sykes, B. D. (1997) *Biochemistry 36*, 12519−12525.
29. Evenäs, J., Malmendal, A., Thulin, E., Carlström, G., and Forsén, S. (1998) *Biochemistry 37*, 13744−13754.
30. Malmendal, A., Evenäs, J., Thulin, E., Gippert, G. P., Drakenberg, T., and Forsén, S. (1998) *J. Biol. Chem. 273*, 28994−29001.
31. Chao, S.-H., Suzuki, Y., Zysk, J. R., and Cheung, W. Y. (1984) *Mol. Pharm. 26*, 75−82.
32. Ohki, S., Iwamoto, U., Aimoto, S., Yazawa, M., and Hikichi, K. (1993) *J. Biol. Chem. 268*, 12388−12392.
33. Pethig, R., Kuhn, M., Payne, R., Adler, E., Chen, T., and Jaffe, L. (1989) *Cell Calcium 10*, 491−498.
34. Aramini, J. M., Drakenberg, T., Hiraoki, T., Ke, Y., Nitta, K., and Vogel, H. J. (1992) *Biochemistry 31*, 6761−6768.
35. Belton, P. S., Cox, I. Y., and Harris, R. K. (1985) *J. Chem. Soc., Faraday Trans. 2 81*, 63−75.
36. McConnell, H. M. (1958) *J. Chem. Phys. 28*, 430−431.
37. Bull, T. E. (1972) *J. Magn. Reson. 8*, 344−353.
38. Bull, T. E., Forsén, S., and Turner, D. (1978) *J. Chem. Phys. 70*, 3106−3111.
39. Halle, B., and Wennerström, H. (1981) *J. Magn. Reson. 44*, 89−100.
40. Wahlgren, M. M., Dejmek, P., and Drakenberg, T. (1993) *J. Dairy Res. 60*, 65−78.
41. Drakenberg, T., Johansson, C., and Forsén, S. (1997) in *Protein NMR Techniques* (Reid, G. G., Ed.) pp 299−323, Humana Press Inc., Totowa, NJ.
42. Zhang, O., Kay, L. E., Oliver, J. P., and Forman-Kay, J. D. (1994) *J. Biomol. NMR 4*, 845−858.
43. Shaka, A. J., Barker, P. B., and Freeman, R. (1985) *J. Magn. Reson. 64*, 547−552.
44. Wishart, D. S., Bigham, C. G., Yao, J., Abildgaard, F., Dyson, H., Oldfield, J., Markley, J. L., and Sykes, B. D. (1995) *J. Biomol. NMR 6*, 135−140.
45. Bryant, D. T. W. (1985) *Biochem. J. 226*, 613−616.
46. Teleman, A., Drakenberg, T., and Forsén, S. (1986) *Biochim. Biophys. Acta 873*, 204−213.
47. Sandström, J. (1982) *Dynamic NMR Spectroscopy*, 1st ed., Academic Press Inc., London.
48. Malmendal, A., Evenäs, J., Forsén, S., and Akke, M. (1999) (manuscript in preparation).
49. Vogel, H. J., Drakenberg, T., Forsén, S., O′Neil, J. D. J., and Hofmann, T. (1985) *Biochemistry 24*, 3870−3876.
50. Reid, R. E., and Procyshyn, R. M. (1995) *Arch. Biochem. Biophys. 323*, 115−119.
51. Pedigo, S., and Shea, M. A. (1995) *Biochemistry 34*, 10676−10689.
52. Peersen, O. B., Madsen, T. S., and Falke, J. J. (1997) *Protein Sci. 6*, 794−807.
53. Kuboniwa, H., Tjandra, N., Grzesiek, S., Ren, H., Klee, C. B., and Bax, A. (1995) *Nat. Struct. Biol. 2*, 768−776.
54. Chattopadhyaya, R., Meador, W. E., Means, A. R., and Quiocho, F. A. (1992) *J. Mol. Biol. 228*, 1177−1192.
55. Ferrin, T. E., Huang, C. C., Jarvis, L. E., and Langridge, R. (1988) *J. Mol. Graphics 6*, 13−27.

BI9909288